HHS Public Access

Author manuscript

Genes Brain Behav. Author manuscript; available in PMC 2018 February 01.

Published in final edited form as:

Genes Brain Behav. 2017 February ; 16(2): 250–259. doi:10.1111/gbb.12327.

A HETEROZYGOUS MUTATION IN TUBULIN, BETA 2B (*TUBB2B*) CAUSES COGNITIVE DEFICITS AND HIPPOCAMPAL DISORGANIZATION

Rolf W. Stottmann[#a,b,c,#], **Ashley Driver**[a], **Arnold Gutierrez**[b,d], **Matthew R. Skelton**[b,d], **Michael Muntifering**[c], **Christopher Stepien**[a], **Luke Knudson**[a], **Matthew Kofron**[c], **Charles V. Vorhees**[#b,d], and **Michael T. Williams**[#b,d]

[a]Division of Human Genetics, Cincinnati Children's Hospital Medical Center, Cincinnati, OH 45229

[b]Graduate Program in Neuroscience, University of Cincinnati College of Medicine, Cincinnati Children's Hospital Medical Center, Cincinnati, OH 45229

[c]Division of Developmental Biology, Cincinnati Children's Hospital Medical Center, Cincinnati, OH 45229

[d]Division of Neurology, Cincinnati Children's Hospital Medical Center, Cincinnati, OH 45229

[#] These authors contributed equally to this work.

Abstract

Development of the mammalian forebrain requires a significant contribution from tubulin proteins to physically facilitate both the large number of mitoses in the neurogenic brain (in the form of mitotic spindles) as well as support cellular scaffolds to guide radial migration (radial glial neuroblasts). Recent studies have identified a number of mutations in human tubulin genes affecting the forebrain, including *TUBB2B*. We previously identified a mouse mutation in *Tubb2b* and we show here that mice heterozygous for this missense mutation in *Tubb2b* have significant cognitive defects in spatial learning and memory. We further showed reduced hippocampal long-term potentiation consistent with these defects. In addition to the behavioral and physiological deficits, we show here abnormal hippocampal morphology. Taken together, these phenotypes suggest that heterozygous mutations in tubulin genes result in cognitive deficits not previously appreciated. This has implications for design and interpretation of genetic testing for humans with intellectual disability disorders.

INTRODUCTION

Tubulin molecules are fundamental building blocks of the cell with particular importance for neuronal morphology and function. In recent years, numerous mutations have been identified in humans with predominantly central nervous system (CNS) deficits. *TUBA4A* is

[#]Correspondence to: Rolf Stottmann, Ph.D., Cincinnati Children's Hospital Medical Center, 3333 Burnet Ave., MLC 7016, Cincinnati, OH 45229, Ph. (513)-636-7136, Fax. (513)-636-4373, rolf.stottmann@cchmc.org.

The authors declare no conflicts of interest.

linked to amyotrophic lateral sclerosis without fronto-temporal dementia (Smith et al., 2014), *TUBB1* mutations have been found in patients with macrothrombocytopenia (Kunishima et al., 2009), and *TUBB4A* variants are associated with dystonia and hypomyelinating leukodystrophy (Hersheson et al., 2013; Lohmann et al., 2013; Simons et al., 2013). The most common findings, however, are with tubulin mutations and malformations of the CNS (Bahi-Buisson et al., 2014; Jaglin and Chelly, 2009; Tischfield et al., 2011). *TUBA1A, TUBA8, TUBB/TUBB5, TUBB2A, TUBB2B, TUBB3,* and *TUBG1* have all been associated with CNS defects such as polymicrogyria, lissencephaly, cortical dysplasia, and congenital fibrosis of the extraocular muscles (Abdollahi et al., 2009; Bahi-Buisson et al., 2014; Breuss et al., 2012; Cederquist et al., 2012; Cushion et al., 2013; Cushion et al., 2014; Jaglin et al., 2009; Jamuar and Walsh, 2014; Keays et al., 2007; Poirier et al., 2007; Romaniello et al., 2012; Stottmann et al., 2013; Tischfield et al., 2010).

We recently reported the only mouse mutant in *Tubb2b.* This allele was recovered from a forward genetic screen designed to identify genes required for normal mammalian forebrain development (Stottmann et al., 2013). The *brain dimple (brdp)* mutation is in a highly conserved amino acid in the fourth exon of TUBB2B. *Tubb2b*$^{brdp/+}$ heterozygote mice are viable while homozygous *Tubb2b*$^{brdp/brdp}$ mutant mice do not survive past birth. We noted hyperactive locomotor patterns in our previous analysis of the *Tubb2b*$^{brdp/+}$ mice and a molecular analysis of the *Tubb2b*$^{brdp/+}$ mouse cerebral cortex indicated a reduction in *Gad1*-positive interneurons, but we had not examined the hippocampus in any detail. Here we further explore the behavior in these mice and show that *Tubb2b*$^{brdp/+}$ mice have cognitive and electrophysiological defects. We also show significant deficits in adult hippocampal structure with a combination of histological and immunohistochemical approaches.

MATERIALS AND METHODS

Animals and Treatments

Adult male mice with heterozygous missense mutations in the *beta tubulin, 2b* gene (*Tubb2b*$^{brdp/+}$) and wildtype (WT) littermates were used as subjects. Only males were used since sex differences in tubulinopathies have not been reported. No more than 1 animal per genotype was used from a litter for behavioral testing to obviate litter effects. For each behavior test reported here, we tested 19 *Tubb2b*$^{brdp/+}$ animals and 19 WT littermates. The mice used in this study were on a mixed genetic background: the mutation was generated on an A/J background and crossed to FVB/NJ for positional cloning. Other than the reduced fecundity and behavioral phenotypes (here and Stottmann et al., 2013), we have not noted any increased morbidity and/or mortality in *Tubb2b*$^{brdp/+}$ animals. To facilitate the behavioral analyses performed here by introducing coat color, the allele was further crossed to C57BL/6J for no more than two generations. In order to determine if this change in genetic background is a confounding variable, we reviewed data from our initial study (Stottmann et al., 2013) and see evidence for the morphological defects we present here in our previously collected animals. This suggests that the altered genetic background is not the root cause of the phenotypes we describe here. We also used the *Thy1-GFP* mouse (*Tg(Thy1-EGFP)M*^{Jrs}*/J*, The Jackson Laboratory, Bar Harbor; Feng et al., 2000) to visualize individual cells within the CNS. The vivarium at Cincinnati Children's Research Foundation

is fully accredited by the Association for the Assessment and Accreditation of Laboratory Animal Care. Euthanasia was performed after isoflurane sedation. The vivarium is pathogen free and uses the Modular Animal Caging System (Alternative Design, Siloam Spring, AR) with HEPA filtered air that was supplied via the Flex-Air System (Alternative Design, Siloam Spring, AR) at 30 air changes/h. Reverse osmosis filtered water was provided continuously with an automated watering system (SE Lab Group, Napa, CA). Each cage had ad libitum autoclaved food, commercial woodchip bedding, and a nestlet to provide partial environmental enhancement. Animals were maintained on a 14 h light: 10 h dark cycle and group housed. All procedures were approved by the Institutional Animal Care and Use Committee of Cincinnati Children's Research Foundation and conform to animal use guidelines set forth by the National Institutes of Health. The *Tubb2b*$^{brdp/+}$ mice are available upon request.

Behavioral Assessment

Animals began behavioral testing between postnatal day (P) 55-60 and completed testing by P120. All animals were sequentially tested in the behaviors described below during the light phase of the light: dark cycle.

Locomotor Activity

On the first day of behavioral testing, animals were assessed in an automated locomotor activity chamber (Photobeam Activity System (PAS), San Diego Instruments, San Diego, CA) for 1 h. Activity chambers were 41 cm (W) × 41 cm (D) × 38 cm (H) with 16 photobeams spaced 2.5 cm apart in the X and Y planes. The dependent measures were the total number of infrared photobeam interruptions (beam breaks) and the number of beam breaks in the peripheral and central regions of the apparatus, as well as repetitive breaks of the same photocell beam as an index of fine motor movement.

Spatial Learning and Memory

Spatial navigation was assessed using the the Morris water maze (MWM). The tank was 122 cm in diameter with a height of 51 cm and was filled with room temperature water (21 ± 1°C) to a level of 31 cm. The platform height was 30.5 cm and the platform size was 10 cm in diameter during acquisition and 7 cm in diameter during reversal. The platform was not visible to the mice because it was colored to match the white background of the maze. In all phases, trials were a maximum of 90 s and animals were tested in a distributed fashion with at least a 10 min intertrial interval (ITI). On day-1, mice were given fixed cued platform training with the platform position and start position held constant for 6 trials to teach the animals the basic parameters of the task and eliminate off-task behavior such as thigmotaxis or jumping off the platform once having found it. A 10 cm diameter platform had a cue (orange ball) mounted on it that protruded 12 cm above the platform on a brass rod to demarcate the platform position. Curtains enclosed the tank during this phase to minimize access to distal cues. Latency to reach the platform was recorded on each trial (video tracking was not possible on these trials because the curtains interfered with tracking accuracy).

Animals were then given acquisition trials for 5 days with curtains open and a 10 cm platform hidden in the SW quadrant and 1 memory (probe) trial with no platform on day-6. During acquisition, four trials were administered each day in a distributed fashion with at least a 10 min ITI with quasi-randomized start positions (N, E, SE, NW) and a time limit of 90 s per trial with 10-15 s on the platform between trials (Vorhees and Williams, 2006). Data were collected using ANY-maze software (Stoelting Instruments, Wood Dale, IL). Animals that did not find the platform within 90 s were removed and placed on the platform for 10-15 s. For the probe trial, animals were started from a novel location (NE position) and allowed 30 s with no platform to determine their search pattern as a measure of reference memory) for where the platform used to be.

Following acquisition, animals were given reversal trials with a 7 cm platform located in the NE quadrant for 5 days with start positions of S, W, NW, SE and 1 probe trial on day-6 with a novel SW start position. All other parameters were the same as for acquisition. The dependent measures on hidden platform trials were path length, swim speed, latency, and path efficiency. Path efficiency is the difference between the shortest path to the platform versus the animal's actual distance. For probe trials, measures were average distance to the previous platform location and percent time in the goal quadrant. Average distance was used because it has been shown to be the most sensitive measure of memory in the MWM (Maei et al., 2009). We also analyzed percent time in the target quadrant.

The final phase was a randomized cued platform procedure. Mice were tested for 5 days, 2 trials per day, with curtains closed around the tank and a marked platform, but for these trials, both the start and platform positions were randomized on every trials. The same platform with an orange ball mounted on it that was used during the training phase was used. Animals were given 90 s per trial as before and provided with at least a 10 min ITI. Latency was again recorded.

Conditioned Fear

Conditioned fear was tested in a three day procedure. On day-1, mice were placed in a test chamber with a speaker mounted on one wall and a grid floor connected to a scrambled foot shock source, and with video camera mounted on the ceiling connected to a computer with Freezeframe software (Coulbourn Instruments, Allentown, PA). The test chamber was located in an outer sound-attenuating chamber. Mice were habituated to the chamber for 10 min before exposure to 3 tone-foot shock pairings (82 dB, 2 kHz, 30 s on/off cycle). Each pairing consisted of a 30 s tone accompanied during the last second by a foot shock (0.3 mA for 1 s) delivered through the floor. Tone-shock pairings were separated by 180 s and freezing (non-movement for > 4 s) was scored at 1 min intervals for the last minute prior to tone-shock pairings and for each minute after the first shock. As a test of contextual fear, on day-2 animals were returned to the chamber for 6 min with no tone or shock presented. Freezing was assessed each minute. On day-3, cued fear was assessed. Animals were placed in the chamber with a novel floor and different lighting. Following 3 min of baseline exploration, the tone was presented for 3 min and freezing scored. Percent time freezing after tone onset relative to the 3 min prior to the tone was analyzed.

Long-term potentiation

The MED64 system was used to assess long-term potentiation (LTP). Briefly, the brains were rapidly removed and transferred to ice cold artificial cerebral spinal fluid (aCSF: 124 mM NaCl, 26mM NaHCO3, 10 mM dextrose 3mM KCl, 1.25 mM NaH2PO4, 2mM CaCl2, and 1mM MgSO4). Horizontal sections (300 μm) at the level of the hippocampus were obtained and placed in oxygenated aCSF at 37° for 1 h. The CA1 region was placed on the upper 16 electrodes, while the dentate was over the lower 40 electrodes, and 8 electrodes were situated in the hippocampal fissure. Sections were transferred to a humidified recording chamber and allowed to acclimate to these conditions until stable baseline field excitatory post-synaptic potentials (fEPSPs) were obtained (approximately 5-10 min). The fEPSPs were recorded following stimulation (60 mA) that was alternately delivered from two stimulus electrodes once every 5 s during a 5 min baseline as well as during the experimental periods. For LTP, a theta burst stimulation of 90 mA was delivered to one of the stimulating electrodes every 200 ms for 2 s for a total of 10 pulses; fEPSPs were examined for 5 min.

Histology and Immunohistochemistry

For both histology and immunohistochemistry (IHC), adult (>4 months of age) *Tubb2b*$^{brdp/+}$ mice and WT littermates were transcardially perfused with heparinized PBS and 4% paraformaldehyde (PFA) solution. Brains were dissected and fixed overnight in 4% PFA followed by either sucrose dehydration and embedding in OCT compound (Tissue-Tek, for IHC) or placed in 70% ethanol and processed for paraffin embedding (and histological analysis). For IHC, citrate buffer antigen retrieval was performed on cryosections, blocked in 5% normal goal serum in PBST, and primary antibodies were inducated overnight. Antibodies used were the neuron specific marker NeuN (1:1000, Chemicon MAB377) or the granule cell marker Calbindin (1:4000, Swant #300) in 5% normal goat serum in PBST. Sections were washed in PBS and incubated in AlexaFluor 488 goat anti-rabbit or goat anti-mouse secondary (1:500, Life Technologies) for 1 h at room temperature followed by incubation in DAPI (1:1000) for 15 min followed by sealing with ProLong gold (Life Technologies). For histology, 5 μm paraffin sections were cut and stained with hematoxylin and eosin (H&E). All paired images are at the same magnification and at least three pairs of samples were assayed for each experiment. Photos were taken on a Zeiss AxioImager. All animals used in histological, Calbindin and NeuN immunohistochemical analyses (Figure 6) were from the cohort that had been previously behaviorally tested.

Quantification of immunohistochemistry

Quantification of NeuN-positive cells was done using Imaris Software (Bitplane). Briefly, images were analyzed (all at the same magnification, n=3 *Tubb2b*$^{+/+}$ and *Tubb2b*$^{brdp/+}$ pairs) by defining an area of NeuN-positive cells from the CA3 to the CA1 region. The number of NeuN-positive cells was then measured per μm^2. Statistical analysis was performed using the student's t-test ($p < 0.05$).

Clearing and Imaging Methods

Hand cut brain sections (roughly 2-3 mm thick) from *Tubb2b*$^{brdp/+}$*;Thy1-GFP* and *Tubb2b*$^{+/+}$*;Thy1-GFP* controls were prepared according to an adapted PACT/RIMS protocol (Yang et al., 2014). After fixation in 4% PFA, the tissue was incubated overnight in 4% acrylamide hydrogel monomer solution. The gel was polymerized at 37 °C for approximately 4 h. Once set, excess hydrogel was decanted and the tissue was washed in 8% SDS at 37°C for several days or until translucent. After several PBS washes, the tissue was placed in RIMS (Refractive Index Matching Solution- 40 g Histodenz in 30 mL 0.2 M phosphate buffer with detergents and anti-fade) and custom-mounted in a coverglass-topped dish. Imaging was performed on a Nikon A1R confocal and on a Nikon FN1 upright microscope. GFP was excited with a 488 nm diode laser and emission was collected using a 525-50 nm bandpass filter. Large overview images (dentate gyrus-CA3) were taken using a 10X Plan Fluor 0.3 NA objective. All images of *Thy1-GFP* animals were acquired using NIS-Elements software in the Confocal Imaging Core at CCHMC. *Tubb2b*$^{brdp/+}$*;Thy1-GFP* and *Tubb2b*$^{+/+}$*;Thy1-GFP* control animals were not from the same cohort as the behavioral testing.

Data Analyses

Data were analyzed using mixed linear factorial analysis of variance (ANOVA; Proc Mixed, SAS v9.3, SAS Institute, Cary, NC) with Kenward-Rogers degrees of freedom (first order) or t-tests for independent samples where appropriate. Between subject factors were genotype (wildtype vs. *Tubb2b*$^{brdp/+}$), and within subject factors were time interval for locomotor activity (5 min intervals) and day for MWM. For conditioned fear, within factors were pre-tone on day-1 vs day-1 percent freezing and for Day-3 it was pre-tone vs tone percent freezing. Litter was treated as a randomized block factor. Significant interactions were further analyzed using slice-effect ANOVAs. Correlations were run using Proc Corr in SAS. Significance was set at $p \leq 0.05$. Behavioral data are presented as least square mean ± least square SEM and histological data as ordinary means ± SEM.

RESULTS

Tubb2b$^{brdp/+}$ mice have increased locomotor activity

Locomotor activity was first assessed in *Tubb2b*$^{brdp/+}$ and control mice to determine exploratory activity and habituation (Amos-Kroohs et al., 2013). No main effect of genotype was observed for total horizontal activity, although there was a trend in agreement with the previous study ($p < 0.10$, Figure 1, top inset). The main effect of time across intervals was significant ($p < 0.001$) and showed that animals exhibited typical patterns of time-dependent habituation (Figure 1, top). There was no significant interaction between genotype and time. For central horizontal activity, there was a significant main effect of genotype, $F(1, 45.7) = 5.96$, $p < 0.02$ (Figure 1, bottom inset) and interval ($p < 0.0001$), but no interaction (Figure 1, bottom). The *Tubb2b*$^{brdp/+}$ mice spent more time in the center than WT mice. For peripheral horizontal activity, there was no significant effect of genotype or the interaction of genotype × interval, but interval was significant ($p < 0.0001$). For repetitive activity, *Tubb2b*$^{brdp/+}$ mice showed no significant differences from WT. Consistent with our previous

results, these data demonstrated only a significant central region increase suggesting reduced anxiety in the *Tubb2b*$^{brdp/+}$ mice compared with WT mice.

Tubb2b$^{brdp/+}$ mice have deficits in spatial learning and memory

Allocentric navigation was assessed in the MWM (Vorhees and Williams, 2006). Prior to testing for spatial learning, mice were given training trials to a visible platform with fixed start and platform position. These training trials greatly reduce nonperformance behaviors such as floating or swimming only in the periphery. During training trials, there were no differences between genotypes on time to locate the platform (WT: 26.6 ± 3.1 s and *Tubb2b*$^{brdp/+}$: 29.5 ± 3.1 s) nor was there an interaction of genotype × trial. A significant trial main effect ($p < 0.0001$) showed that all mice improved across trials. In order to show that mice started out the MWM with no preexisting differences in swimming ability, we also examined the first trial of cued training only and found no differences (WT: 50.9 ± 6.4 s and *Tubb2b*$^{brdp/+}$: 46.4 ± 6.4 s). Therefore we conclude all mice learned that the platform was the escape and was not near the edge of the tank. This also showed that the mice could see the platform and use it as a cue, and had equal swimming ability with no preexisting differences.

Mice were next tested for allocentric navigation to a hidden platform on acquisition trials in the MWM. During this phase, *Tubb2b*$^{brdp/+}$ mice had slower swim speeds than WT mice, $F(1, 28.4) = 19.6$, $p < 0.0001$, and it should be noted that no issues with floating were observed. There was also an interaction that showed that the groups differed on days 1-3 then converged on days 4 and 5 (Figure 2G; genotype × day: $F(4, 137) = 2.68$, $p < 0.04$. *Tubb2b*$^{brdp/+}$ mice had longer latencies to reach the platform than WT mice, $F(1, 34.8) = 27.79$, $p < 0.0001$ (Figure 2E). Because of the swim speed effect and to reduce any potential influence on latency, we analyzed path length and path efficiency. There was a significant effect of genotype on path length in *Tubb2b*$^{brdp/+}$ mice compared with WT mice, $F(1, 40.2) = 6.96$, $p < 0.02$ (Figure 2C). For path efficiency, there was also a significant effect of genotype, $F(1,54.3) = 12.43$, $p < 0.001$, but no interaction between genotype and day (Figure 2A). The effect of day was also significant for latency ($p < 0.0003$), path length ($p < 0.0001$), and path efficiency ($p < 0.0001$). We next investigated if failed trials influenced the outcome of the various dependent measures. We observed that if animals failed on a trial in this task it was more likely to occur on day 1 and then sporadically on the other days. However, an analysis of each of the dependent measures with failed trials removed did not change the outcome. On the acquisition probe trial, there were no differences in swim speed ($p < 0.08$), however *Tubb2b*$^{brdp/+}$ mice had greater average distance from the platform site $F(1, 18) = 7.02$, $p < 0.02$ (Figure 3A) and decreased percent time in the target quadrant compared with WT mice, $F(1, 18) = 6.64$, $p < 0.02$ (WT: 26.3 ± 3.7% vs *Tubb2b*$^{brdp/+}$ 14.2 ± 3.7%).

Following acquisition, the platform was relocated to the opposite quadrant and mice were tested on reversal trials to assess new learning. During this phase, there again was a difference in swim speed between genotypes, $F(1, 30.2) = 5.08$, $P < 0.04$, (Figure 2H), however the effect had disappeared by day-5. *Tubb2b*$^{brdp/+}$ mice had longer latencies, $F(1, 30.3) = 19.74$, $p < 0.0001$ (Figure 2F), path lengths (Figure 2D) , $F(1, 38.3) = 9.62$, $p <$

0.004, and reduced path efficiency ($F(1,38.9) = 21.19$, $p < 0.0001$) compared with WT mice (Figure 2B). Significance still remained if trials were analyzed after the removal of failed trials. The effect of Day was significant for latency ($p < 0.004$), path length ($p < 0.0001$), and path efficiency ($p < 0.001$); there were no genotype × day interactions for these measures. On the reversal probe trials, no swim speed differences were found. There were also no effects for average distance to the platform site (Figure 3B) or percent time in the target quadrant (WT: 20.9 ± 3.7 % vs *Tubb2b*$^{brdp/+}$ 13.4 ± 3.7 %).

Following reversal, mice were given random cued platform trials, where the platform and start position were changed on every trial and the goal marked with the pole and plastic ball mounted on the platform as during training and curtains closed around the maze to obscure distal cues. There were genotype, $F(1, 35.5) = 9.97$, $p < 0.004$, and day ($p < 0.002$) main effects but no genotype × day interaction (Figure 4). *Tubb2b*$^{brdp/+}$ mice had longer latencies to locate the platform compared with WT mice, (*Tubb2b*$^{brdp/+}$: 12.7 ± 1.5 s vs WT: 8.4 ± 1.5 s).

To determine how swim speed was related to latency, path length, and path efficiency Pearson correlation coefficients were determined. For the acquisition phase learning trials, the correlation between speed and latency was −0.51 ($p < 0.0001$), between speed and path length it was 0.15 ($p < 0.04$), and between speed and path efficiency it was −0.04 ($p > 0.56$). This shows that swim speed and latency are related (inversely) as would be expected, whereas there is little relationship between speed and path length and no relationship between speed and path efficiency, showing that the effects on the latter two indices reflect differences in spatial learning rather than in performance factors. For reversal phase learning trials, a similar pattern was found, i.e., the correlation between speed and latency was −0.30 ($p < 0.0001$), between speed and path length it was 0.36 ($p < 0.0001$), and between speed and path efficiency it was −0.15 ($p < 0.05$).

Tubb2b$^{brdp/+}$ mice have conditioned fear deficits

On day-1, animals began with an exploratory phase after which they received shock-tone pairings and freezing was assessed. On day-1, the main effect of genotype was not significant, $F(1, 48.3) = 3.53$, $p < 0.07$; interval was significant ($p < 0.0001$), but the interaction was not. *Tubb2b*$^{brdp/+}$ mice were not different in freezing prior to or following shock-tone pairings compared with WT mice (percent time freezing during shock-tone: WT = 44.8 ± 3.1% and *Tubb2b*$^{brdp/+}$ = 34.3 ± 3.2%). On day-2, mice were placed back in the chamber without shock or tone and freezing was examined to determine if they remembered the context in which they were shocked; a hippocampus-dependent response. The *Tubb2b*$^{brdp/+}$ mice showed less freezing than the WT mice, $F(1, 15.8) = 9.98$, $p < 0.007$ (percent time freezing: WT = 38.2 ± 3.7% and *Tubb2b*$^{brdp/+}$ = 22.7 ± 3.8%). On day-3, animals were placed in a new environment for 3 min of exploration and then presented with the tone for another 3 min (with no shock) and the difference between the first and second 3 min analyzed. There was no effect of genotype or interaction of genotype × interval; interval was significant ($p<0.0001$). There were no differences between the *Tubb2b*$^{brdp/+}$ mice and WT mice prior to or following the tone presentation (percent time freezing following tone:

WT = 70.4 ± 4.7% and *Tubb2b*$^{brdp/+}$ = 66.2 ± 4.5%) indicating no deficit in cued fear conditioning.

Tubb2b$^{brdp/+}$ heterozygotes have reduced long-term potentiation

LTP in the CA1 region of the hippocampus is a cellular correlate of spatial learning and memory (Pavlides et al., 1991). Using multi-electrode arrays, LTP was evaluated in the CA1 region of *Tubb2b*$^{brdp/+}$ mice in order to determine if the learning deficits observed were accompanied by deficits in synaptic plasticity. Following the establishment of stable baseline fEPSP responses, LTP was induced using a theta burst stimulus (TBS). Increases in fEPSP slope and amplitude were observed for both WT and *Tubb2b*$^{brdp/+}$ mice, consistent with the induction of LTP. The amplitude and slope of the fEPSPs were significantly blunted in the CA1 region of *Tubb2b*$^{brdp/+}$ mice compared with WT mice (Figure 5) following TBS, confirming that *Tubb2b* mutations impair LTP. This suggests that Tubb2b alters synaptic plasticity in a way that could be the underlying cause of the learning deficits observed. Time × gene interactions were not observed in either slope or amplitude following TBS (for slope: $F(178,1246)=0.29$, $p < 1$), suggesting the reduction in LTP was throughout the assessment period and did not show a separate effect on LTP induction versus maintenance.

Tubb2b$^{brdp/+}$ mice have disrupted hippocampal morphology

Since *Tubb2b*$^{brdp/+}$ mice have deficits in learning and memory of the type associated with the hippocampus, as well as CA1-mediated LTP deficits, we performed a molecular analysis for hippocampal morphological changes. Hematoxylin and eosin (H&E) staining showed neuronal disorganization and heterotopic areas in the CA3 region of the *Tubb2b*$^{brdp/+}$ mice compared with WT mice (Figure 6 A-D). The nuclei in the *Tubb2b*$^{brdp/+}$ mice were more dispersed than in control, where an organized stream of nuclei extend beyond the lateral extent of the blades of the dentate gyrus. Immunostaining for Calbindin, which is immunoreactive in mossy fiber tracts, indicated disorganized fibers compared with controls (Figure 6E,F). NeuN staining for differentiated neurons confirmed the pyramidal cell staining profile within the CA3 region was reduced in the *Tubb2b*$^{brdp/+}$ animals compared with controls (Figure 6 G,H, quantified in I).

We further analyzed hippocampal morphology and connectivity by crossing *Tubb2b*$^{brdp/+}$ mice with mice carrying the Thy1-GFP transgene that distinctly labels subsets of neurons in the developing CNS (Feng et al., 2000). GFP staining in 4 month old animals showed mossy fiber projections extending from the dentate gyrus to two distinct populations in WT mice (Figure 7A). The suprapyramidal bundle (SPB) is restricted to an area above the CA3 pyramidal neurons, whereas the infrapyramidal bundle (IPB) is below this cell layer. In *Tubb2b*$^{brdp/+}$ animals the mossy fibers were intermingled with the pyramidal layer obscuring the clear separation between SPB and IPB areas (Figure 7B). Together, these data indicate that the circuitry of the adult hippocampus is not properly established and functional in animals heterozygous for the *Tubb2b*$^{brdp/+}$ mutation. These morphological phenotypes are consistent with at least contributing to the behavior deficits we describe above.

DISCUSSION

The data presented here demonstrate that a heterozygous *Tubb2b*$^{brdp/+}$ mutation in mice leads to significant spatial learning and memory reductions and conditioned contextual, but not cued, fear deficits. These were associated at the cellular level with both electrophysiological and histological changes. We also found increased central locomotor activity differences suggesting altered anxiety. In agreement with the previous study (Stottmann et al., 2013), the mice showed mild hyperactivity, although this did not reach the level of significance in this experiment. For the learning deficits, these were found on acquisition learning and on reversal trials when the platform was moved to a new location, as well as contextual fear, and therefore implicate the hippocampus as an affected region for these deficits. Reduced LTP further implicated hippocampal involvement in the *Tubb2b*$^{brdp/+}$ phenotype. Consistent with these findings, we observed anatomical defects in *Tubb2b*$^{brdp/+}$ mice in the hippocampus that provide further converging evidence for disrupted neuronal migration in the developing hippocampus.

The allocentric learning and memory reductions observed in *Tubb2b*$^{brdp/+}$ mice during MWM testing also reduced swim speed, and raises the issue of whether the deficits were central or peripheral, i.e., resulting from a performance effect that has nothing to do with hippocampally mediated spatial navigation or were, in fact, cognitive deficits. While it might be possible that performance differences in locomotor performance in a novel environment or swim ability might account for some of the cognitive differences, one would expect that these differences would consistently be present. To address this, we analyzed the data several ways in order to isolate the effects on learning versus those on performance. First, in the MWM the *Tubb2b*$^{brdp/+}$ mice had similar swimming times on the cued training trials as did the WT mice and, importantly, did not show any difference in latency to the cued platform on the first trial. Second, we found that latency on training trials did not differ between genotypes, indicating that the genotypes were not different when they entered the hidden platform acquisition phase. During acquisition, direct measurements of swim speed showed that *Tubb2b*$^{brdp/+}$ mice swam slower, but this effect was dependent on day and dissipated across days such that they were not different from WT mice on later days when path length and path efficiency showed the largest differences. Moreover, on the acquisition probe trial, both groups showed no significant differences in swim speed but did differ on distance to the former platform site and on percent time in the target quadrant. When the platform was moved for reversal testing, *Tubb2b*$^{brdp/+}$ mice again swam slower and had longer path lengths and reduced path efficiency. When we examined correlations between measures on acquisition and reversal, we saw that while swim speed was correlated inversely with latency, speed has only a small correlation with path length and was not correlated with path efficiency. On the reversal probe trial, no differences were found on swim speed or measures of memory. Since there was evidence of memory impairment on the acquisition probe trial, and no swim speed differences and no memory impairment on the reversal probe trials and no swim speed differences, it is apparent that swim speed and memory assessed by average distance to the platform site and quadrant preference are not related to swim speed. During cued random trials given last, *Tubb2b*$^{brdp/+}$ showed a reduction in swim speed but the effect was small (*c.f.* Figure. 2E,F vs. Figure. 3 shown on the same scale). When swim speed is

examined as a function of day, it is evident that the *Tubb2b*$^{brdp/+}$ mice begin each new phase swimming slower and then caught up to WT mice, whereas the opposite was seen for path length and path efficiency where the groups started equally and then diverged. Together, these data show that *Tubb2b*$^{brdp/+}$ mice simultaneously have a small performance effect and a larger cognitive deficit that is not accounted for by swim speed differences. While we did observe slight hyperactivity that might contribute to reduced freezing in the conditioned fear test, it should be noted that no significant differences were observed in the *Tubb2b*$^{brdp/+}$ mice on Day 1 or Day 3 of conditioned fear. The fact that a difference was observed only on Day 2 when contextual memory was assessed shows that the hippocampus-dependent pattern of effects remained consistent between the MWM and the conditioned fear.

Mutations affecting both α- and β- tubulin isoforms have been implicated in human patients with axon guidance defects (Liu and Dwyer, 2014). Axon guidance defects are present in the *Tubb2b*$^{brdp/+}$ hippocampus where mossy fibers of the IPB and SPB fail to segregate as these bundles form around the somata of the CA3 pyramidal neurons. It has been shown that the size of the IPB can alter behavioral outputs such special memory in mice (Schwegler et al., 1990). Furthermore, increased mossy fiber projections to the IPB region has been associated with learning deficits in mice deficient for the *creatine kinase, brain* gene (Jost et al., 2002). Additionally, increased mossy fiber tracts may be indicative of increased seizure activity in the brains of *Tubb2b*$^{brdp/+}$ mice (Romer et al., 2011). Here we report both alterations in spatial memory and corresponding changes in the IPB in the *Tubb2b*$^{brdp/+}$ hippocampus. A more extended analysis of hippocampal circuity in the *Tubb2b*$^{brdp/+}$ hippocampus and the developmental origins of these phenotypes will be exciting areas of future research.

A previously identified mouse model of tubulinopathies is the *Tuba1a*$^{Jna/+}$ mouse, an ENU-induced mutation leading to impaired cortical and hippocampal migration and lamination (Keays et al., 2007). The changes we observe in the *Tubb2b*$^{brdp/+}$ mice are similar to those *Tuba1a*$^{Jna/+}$ phenotypes (Keays et al., 2007). However, there are differences in specifics of the cellular hippocampal phenotypes between the two models (Keays et al., 2010). For example, in the *Tuba1a*$^{Jna/+}$ hippocampus the pyramidal cells are disorganized throughout the CA1-CA3 region whereas this disorganization is restricted to CA3 region in the *Tubb2b*$^{brdp/+}$ mouse. Migration of the CA3 pyramidal cells occurs after that of the CA1 region, further suggesting that while these models are similar there are clearly different consequences for hippocampal development (Hayashi et al., 2015). These differences are consistent with the idea that tubulin mutations collectively lead to CNS disorders of migration and axon extension but that mutations in individual tubulin genes have distinct phenotypes. However, as the number of tubulin mutations identified in human cortical malformations increases, the phenotypes appear to be more a spectrum of disorders within the tubulinopathies, rather than a series of distinct genotype-phenotype correlations (Bahi-Buisson et al., 2014; Cushion et al., 2013). Unifying findings for tubulinopathies are cortical migration defects such as polymicrogyria and dysmorphic basal ganglia (Amrom et al., 2014). The results of our data indicate that *TUBB2B* might be considered for analysis in human patients with neurodevelopmental and/or cognitive phenotypes as well as the classicaly associated structural malformations. The emerging literature on tubulinopathies further suggests the gene family as a whole is worth considering in genetic studies of reduced intellectual function.

ACKNOWLEDGEMENTS

This work is supported by the NIH (R01NS085023 to R.W.S., T32ES007051 to C.V.V.) and the Cincinnati Children's Research Foundation.

REFERENCES

Abdollahi MR, Morrison E, Sirey T, Molnar Z, Hayward BE, Carr IM, Springell K, Woods CG, Ahmed M, Hattingh L, Corry P, Pilz DT, Stoodley N, Crow Y, Taylor GR, Bonthron DT, Sheridan E. Mutation of the variant alpha-tubulin TUBA8 results in polymicrogyria with optic nerve hypoplasia. Am J Hum Genet. 2009; 85:737–744. [PubMed: 19896110]

Amos-Kroohs RM, Williams MT, Braun AA, Graham DL, Webb CL, Birtles TS, Greene RM, Vorhees CV, Pisano MM. Neurobehavioral phenotype of C57BL/6J mice prenatally and neonatally exposed to cigarette smoke. Neurotoxicology and teratology. 2013; 35:34–45. [PubMed: 23314114]

Amrom D, Tanyalcin I, Verhelst H, Deconinck N, Brouhard GJ, Decarie JC, Vanderhasselt T, Das S, Hamdan FF, Lissens W, Michaud JL, Jansen AC. Polymicrogyria with dysmorphic basal ganglia? Think tubulin! Clinical genetics. 2014; 85:178–183. [PubMed: 23495813]

Bahi-Buisson N, Poirier K, Fourniol F, Saillour Y, Valence S, Lebrun N, Hully M, Bianco CF, Boddaert N, Elie C, Lascelles K, Souville I, Consortium LI-T, Beldjord C, Chelly J. The wide spectrum of tubulinopathies: what are the key features for the diagnosis? Brain : a journal of neurology. 2014; 137:1676–1700. [PubMed: 24860126]

Breuss M, Heng JI, Poirier K, Tian G, Jaglin XH, Qu Z, Braun A, Gstrein T, Ngo L, Haas M, Bahi-Buisson N, Moutard ML, Passemard S, Verloes A, Gressens P, Xie Y, Robson KJ, Rani DS, Thangaraj K, Clausen T, Chelly J, Cowan NJ, Keays DA. Mutations in the beta-tubulin gene TUBB5 cause microcephaly with structural brain abnormalities. Cell Rep. 2012; 2:1554–1562. [PubMed: 23246003]

Cederquist GY, Luchniak A, Tischfield MA, Peeva M, Song Y, Menezes MP, Chan WM, Andrews C, Chew S, Jamieson RV, Gomes L, Flaherty M, Grant PE, Gupta ML Jr. Engle EC. An inherited TUBB2B mutation alters a kinesin-binding site and causes polymicrogyria, CFEOM and axon dysinnervation. Human molecular genetics. 2012; 21:5484–5499. [PubMed: 23001566]

Cushion TD, Dobyns WB, Mullins JG, Stoodley N, Chung SK, Fry AE, Hehr U, Gunny R, Aylsworth AS, Prabhakar P, Uyanik G, Rankin J, Rees MI, Pilz DT. Overlapping cortical malformations and mutations in TUBB2B and TUBA1A. Brain : a journal of neurology. 2013; 136:536–548. [PubMed: 23361065]

Cushion TD, Paciorkowski AR, Pilz DT, Mullins JG, Seltzer LE, Marion RW, Tuttle E, Ghoneim D, Christian SL, Chung SK, Rees MI, Dobyns WB. De novo mutations in the beta-tubulin gene TUBB2A cause simplified gyral patterning and infantile-onset epilepsy. Am J Hum Genet. 2014; 94:634–641. [PubMed: 24702957]

Feng G, Mellor RH, Bernstein M, Keller-Peck C, Nguyen QT, Wallace M, Nerbonne JM, Lichtman JW, Sanes JR. Imaging neuronal subsets in transgenic mice expressing multiple spectral variants of GFP. Neuron. 2000; 28:41–51. [PubMed: 11086982]

Hayashi K, Kubo K, Kitazawa A, Nakajima K. Cellular dynamics of neuronal migration in the hippocampus. Front Neurosci. 2015; 9:135. [PubMed: 25964735]

Hersheson J, Mencacci NE, Davis M, MacDonald N, Trabzuni D, Ryten M, Pittman A, Paudel R, Kara E, Fawcett K, Plagnol V, Bhatia KP, Medlar AJ, Stanescu HC, Hardy J, Kleta R, Wood NW, Houlden H. Mutations in the autoregulatory domain of beta-tubulin 4a cause hereditary dystonia. Ann Neurol. 2013; 73:546–553. [PubMed: 23424103]

Jaglin XH, Chelly J. Tubulin-related cortical dysgeneses: microtubule dysfunction underlying neuronal migration defects. Trends in genetics : TIG. 2009; 25:555–566. [PubMed: 19864038]

Jaglin XH, Poirier K, Saillour Y, Buhler E, Tian G, Bahi-Buisson N, Fallet-Bianco C, Phan-Dinh-Tuy F, Kong XP, Bomont P, Castelnau-Ptakhine L, Odent S, Loget P, Kossorotoff M, Snoeck I, Plessis G, Parent P, Beldjord C, Cardoso C, Represa A, Flint J, Keays DA, Cowan NJ, Chelly J. Mutations in the beta-tubulin gene TUBB2B result in asymmetrical polymicrogyria. Nature genetics. 2009; 41:746–752. [PubMed: 19465910]

Jamuar SS, Walsh CA. Somatic mutations in cerebral cortical malformations. N Engl J Med. 2014; 371:2038.

Jost CR, Van Der Zee CE, In 't Zandt HJ, Oerlemans F, Verheij M, Streijger F, Fransen J, Heerschap A, Cools AR, Wieringa B. Creatine kinase B-driven energy transfer in the brain is important for habituation and spatial learning behaviour, mossy fibre field size and determination of seizure susceptibility. Eur J Neurosci. 2002; 15:1692–1706. [PubMed: 12059977]

Keays DA, Cleak J, Huang GJ, Edwards A, Braun A, Treiber CD, Pidsley R, Flint J. The role of Tuba1a in adult hippocampal neurogenesis and the formation of the dentate gyrus. Developmental neuroscience. 2010; 32:268–277. [PubMed: 21041996]

Keays DA, Tian G, Poirier K, Huang GJ, Siebold C, Cleak J, Oliver PL, Fray M, Harvey RJ, Molnar Z, Pinon MC, Dear N, Valdar W, Brown SD, Davies KE, Rawlins JN, Cowan NJ, Nolan P, Chelly J, Flint J. Mutations in alpha-tubulin cause abnormal neuronal migration in mice and lissencephaly in humans. Cell. 2007; 128:45–57. [PubMed: 17218254]

Kunishima S, Kobayashi R, Itoh TJ, Hamaguchi M, Saito H. Mutation of the beta1-tubulin gene associated with congenital macrothrombocytopenia affecting microtubule assembly. Blood. 2009; 113:458–461. [PubMed: 18849486]

Liu G, Dwyer T. Microtubule dynamics in axon guidance. Neurosci Bull. 2014; 30:569–583. [PubMed: 24968808]

Lohmann K, Wilcox RA, Winkler S, Ramirez A, Rakovic A, Park JS, Arns B, Lohnau T, Groen J, Kasten M, Bruggemann N, Hagenah J, Schmidt A, Kaiser FJ, Kumar KR, Zschiedrich K, Alvarez-Fischer D, Altenmuller E, Ferbert A, Lang AE, Munchau A, Kostic V, Simonyan K, Agzarian M, Ozelius LJ, Langeveld AP, Sue CM, Tijssen MA, Klein C. Whispering dysphonia (DYT4 dystonia) is caused by a mutation in the TUBB4 gene. Ann Neurol. 2013; 73:537–545. [PubMed: 23595291]

Maei HR, Zaslavsky K, Teixeira CM, Frankland PW. What is the Most Sensitive Measure of Water Maze Probe Test Performance? Front Integr Neurosci. 2009; 3:4. [PubMed: 19404412]

Pavlides C, Westlind-Danielsson AI, Nyborg H, McEwen BS. Neonatal hyperthyroidism disrupts hippocampal LTP and spatial learning. Experimental brain research. 1991; 85:559–564. [PubMed: 1915710]

Poirier K, Keays DA, Francis F, Saillour Y, Bahi N, Manouvrier S, Fallet-Bianco C, Pasquier L, Toutain A, Tuy FP, Bienvenu T, Joriot S, Odent S, Ville D, Desguerre I, Goldenberg A, Moutard ML, Fryns JP, van Esch H, Harvey RJ, Siebold C, Flint J, Beldjord C, Chelly J. Large spectrum of lissencephaly and pachygyria phenotypes resulting from de novo missense mutations in tubulin alpha 1A (TUBA1A). Hum Mutat. 2007; 28:1055–1064. [PubMed: 17584854]

Romaniello R, Tonelli A, Arrigoni F, Baschirotto C, Triulzi F, Bresolin N, Bassi MT, Borgatti R. A novel mutation in the beta-tubulin gene TUBB2B associated with complex malformation of cortical development and deficits in axonal guidance. Developmental medicine and child neurology. 2012; 54:765–769. [PubMed: 22591407]

Romer B, Krebs J, Overall RW, Fabel K, Babu H, Overstreet-Wadiche L, Brandt MD, Williams RW, Jessberger S, Kempermann G. Adult hippocampal neurogenesis and plasticity in the infrapyramidal bundle of the mossy fiber projection: I. Co-regulation by activity. Front Neurosci. 2011; 5:107. [PubMed: 21991243]

Schwegler H, Crusio WE, Brust I. Hippocampal mossy fibers and radial-maze learning in the mouse: a correlation with spatial working memory but not with non-spatial reference memory. Neuroscience. 1990; 34:293–298. [PubMed: 2333144]

Simons C, Wolf NI, McNeil N, Caldovic L, Devaney JM, Takanohashi A, Crawford J, Ru K, Grimmond SM, Miller D, Tonduti D, Schmidt JL, Chudnow RS, van Coster R, Lagae L, Kisler J, Sperner J, van der Knaap MS, Schiffmann R, Taft RJ, Vanderver A. A de novo mutation in the beta-tubulin gene TUBB4A results in the leukoencephalopathy hypomyelination with atrophy of the basal ganglia and cerebellum. Am J Hum Genet. 2013; 92:767–773. [PubMed: 23582646]

Smith BN, Ticozzi N, Fallini C, Gkazi AS, Topp S, Kenna KP, Scotter EL, Kost J, Keagle P, Miller JW, Calini D, Vance C, Danielson EW, Troakes C, Tiloca C, Al-Sarraj S, Lewis EA, King A, Colombrita C, Pensato V, Castellotti B, de Belleroche J, Baas F, ten Asbroek AL, Sapp PC, McKenna-Yasek D, McLaughlin RL, Polak M, Asress S, Esteban-Perez J, Munoz-Blanco JL, Simpson M, Consortium S, van Rheenen W, Diekstra FP, Lauria G, Duga S, Corti S, Cereda C, Corrado L, Soraru G, Morrison KE, Williams KL, Nicholson GA, Blair IP, Dion PA, Leblond CS,

Rouleau GA, Hardiman O, Veldink JH, van den Berg LH, Al-Chalabi A, Pall H, Shaw PJ, Turner MR, Talbot K, Taroni F, Garcia-Redondo A, Wu Z, Glass JD, Gellera C, Ratti A, Brown RH Jr. Silani V, Shaw CE, Landers JE. Exome-wide rare variant analysis identifies TUBA4A mutations associated with familial ALS. Neuron. 2014; 84:324–331. [PubMed: 25374358]

Stottmann RW, Donlin M, Hafner A, Bernard A, Sinclair DA, Beier DR. A mutation in Tubb2b, a human polymicrogyria gene, leads to lethality and abnormal cortical development in the mouse. Human molecular genetics. 2013; 22:4053–4063. [PubMed: 23727838]

Tischfield MA, Baris HN, Wu C, Rudolph G, Van Maldergem L, He W, Chan WM, Andrews C, Demer JL, Robertson RL, Mackey DA, Ruddle JB, Bird TD, Gottlob I, Pieh C, Traboulsi EI, Pomeroy SL, Hunter DG, Soul JS, Newlin A, Sabol LJ, Doherty EJ, de Uzcategui CE, de Uzcategui N, Collins ML, Sener EC, Wabbels B, Hellebrand H, Meitinger T, de Berardinis T, Magli A, Schiavi C, Pastore-Trossello M, Koc F, Wong AM, Levin AV, Geraghty MT, Descartes M, Flaherty M, Jamieson RV, Moller HU, Meuthen I, Callen DF, Kerwin J, Lindsay S, Meindl A, Gupta ML Jr. Pellman D, Engle EC. Human TUBB3 mutations perturb microtubule dynamics, kinesin interactions, and axon guidance. Cell. 2010; 140:74–87. [PubMed: 20074521]

Tischfield MA, Cederquist GY, Gupta ML Jr. Engle EC. Phenotypic spectrum of the tubulin-related disorders and functional implications of disease-causing mutations. Current opinion in genetics & development. 2011; 21:286–294. [PubMed: 21292473]

Vorhees CV, Williams MT. Morris water maze: procedures for assessing spatial and related forms of learning and memory. Nature protocols. 2006; 1:848–858. [PubMed: 17406317]

Yang B, Treweek JB, Kulkarni RP, Deverman BE, Chen CK, Lubeck E, Shah S, Cai L, Gradinaru V. Single-cell phenotyping within transparent intact tissue through whole-body clearing. Cell. 2014; 158:945–958. [PubMed: 25088144]

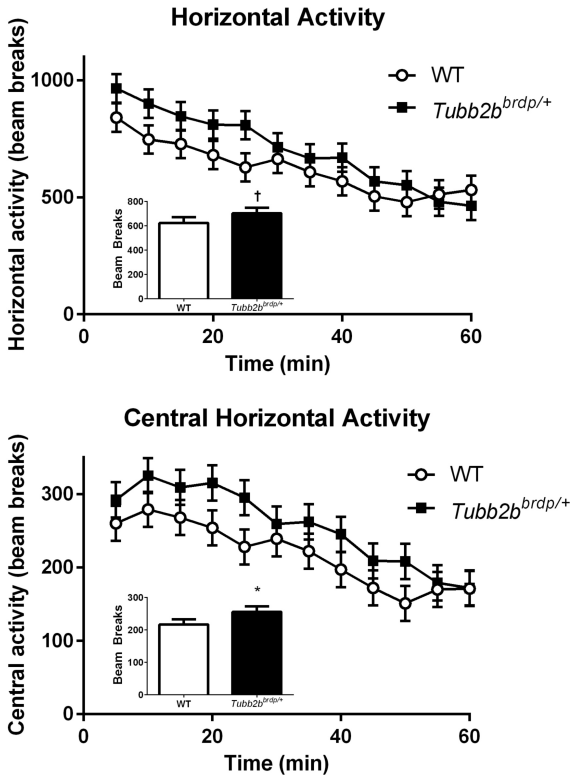

Figure 1. *Tubb2b*$^{brdp/+}$ heterozygous mice exhibit increased locomotion

Horizontal activity (beam breaks) over the 60 min interval are shown in the top panel with the main effect in the inset. Central horizontal activity (beam breaks) over the 60 min interval are shown in the bottom panel with the main effect in the inset. Data are LS Mean ± SEM. * $p < 0.05$, $^{\dagger}p < 0.1$ vs. WT. WT: n = 19 mice; Tubb2b$^{brdp/+}$: n = 19 mice

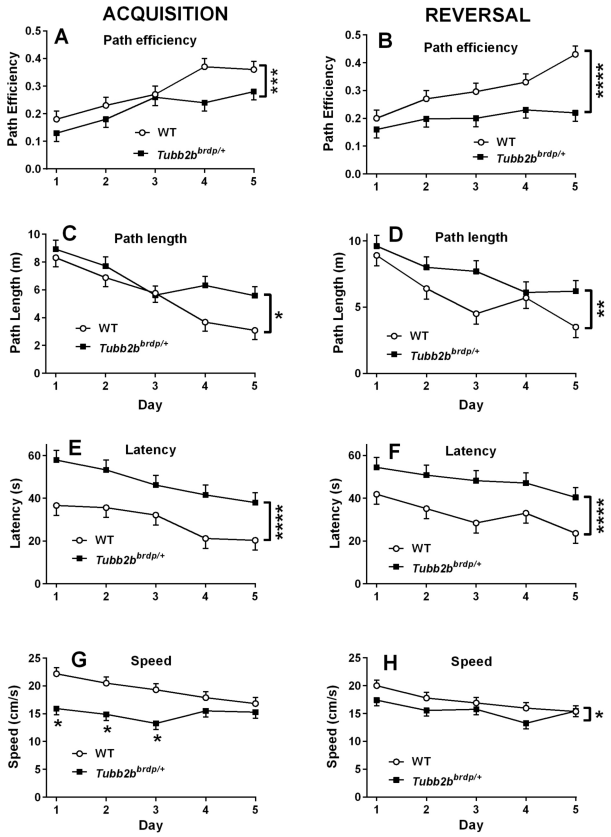

Figure 2. *Tubb2b*$^{brdp/+}$ heterozygous mice exhibit learning deficits

Morris water maze (MWM) acquisition (A,C,E,G) and MWM reversal (B,D,F,H) for path efficiency, path length, latency, and swim speed, respectively. Data are LS Mean ± SEM. * p < 0.05, **p < 0.01, ***p < 0.001, ****p < 0.0001 for main effect vs. WT. WT: n = 19 mice; Tubb2b$^{brdp/+}$: n = 19 mice

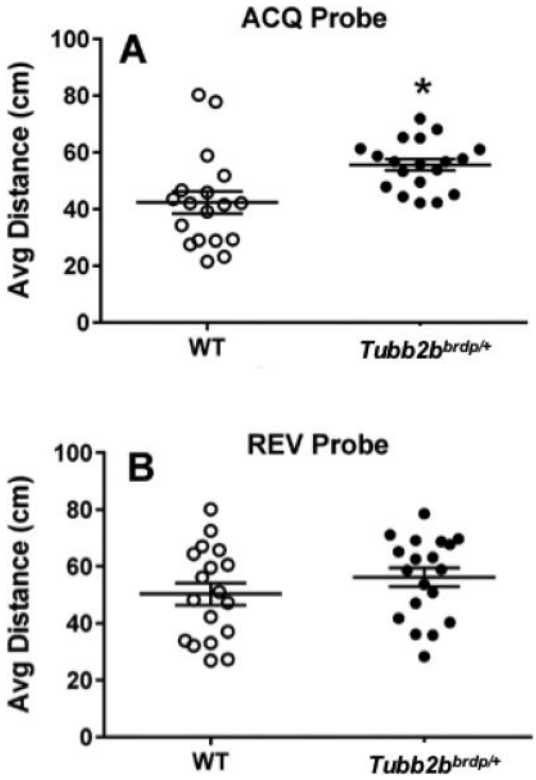

Figure 3. *Tubb2b*$^{brdp/+}$ heterozygous mice exhibit memory deficits

MWM probe trials for average distance to the former platform location given 24 h after the last platform trial of each phase. A, acquisition probe; B, reversal probe. Data are LS Mean ± SEM plus individual data points. *$p < 0.05$ vs. WT. WT: n = 19 mice; Tubb2b$^{brdp/+}$: n = 19 mice

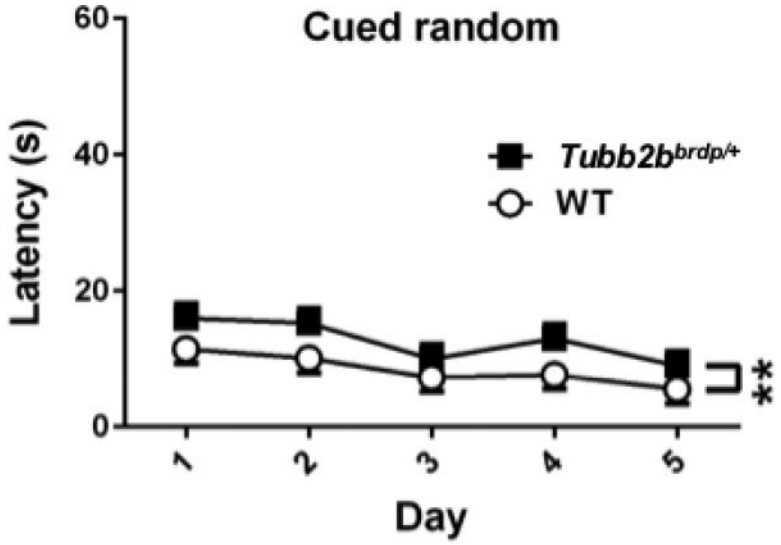

Figure 4. ***Tubb2b*$^{brdp/+}$ heterozygous mice exhibit cued trials**

MWM cued random trials as a test of proximal cue learning (latency, s). There was a significant genotype effect but no interaction. The effect is shown on the same scale as latency in Figure 1 for comparison. As can be seen the latency effect on cued trials was small and did not change across days. **p < 0.01 vs. WT. WT: n = 18 mice; Tubb2b$^{brdp/+}$: n = 18 mice (1 litter was inadvertently missed)

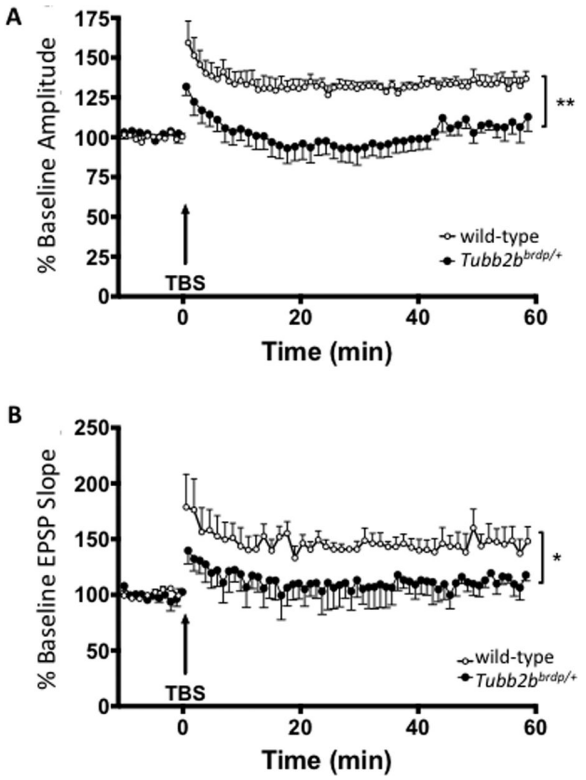

Figure 5. *Tubb2b*$^{brdp/+}$ heterozygous mice have reduced long-term potentiation

Electrophysiological analyses of long-term potentiation (LTP). The amplitude (A) and slope (B) of resulting EPSPs from the parasagittal sections (350 μm) of hippocampal CA1 region were recorded. Both the baseline amplitude and slopes of the EPSP (LTP) in 35 days Tubb2b$^{brdp/+}$ (black circle) was significantly (p= 0.0016 for amplitude and p=0.0419 for slope) decreased compared with WT (open circle) mice after recording for 60 min following stimulation. WT,n = 4 mice; Tubb2b$^{brdp/+}$, n = 4 mice. **p<0.01, *p<0.05.

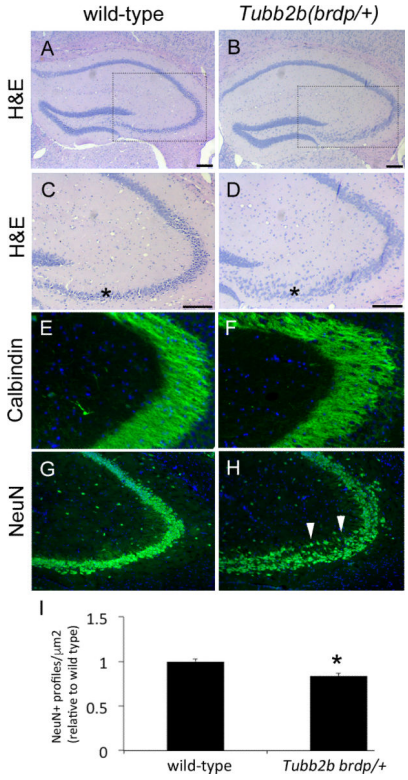

Figure 6. *Tubb2b*$^{brdp/+}$ heterozygous mice have abnormal hippocampal structure

(A-D) Histological analysis revealed hippocampal phenotypes in the CA3 region of heterozygous mice. C,D are higher magnification of approximate areas indicated in A,B. Note the disorganized and dispersed appearance of cells in the CA3 region of the heterozygous animal relative to control (asterisks). (E,F) Immunohistochemistry for Calbindin shows disorganization of fibers in CA3 region with a web-like appearance in the heterozygous animals (arrows). (G,H) NeuN immunohistochemistry further demonstrates disorganization of the CA3 region in the heterozygous animals with a number of ectopic cells (arrow heads). (I) Quantification of NeuN staining shows that there is a reduced staining profile density in the heterozygous animals relative to wild-type (*$p<0.05$, $n=3$).

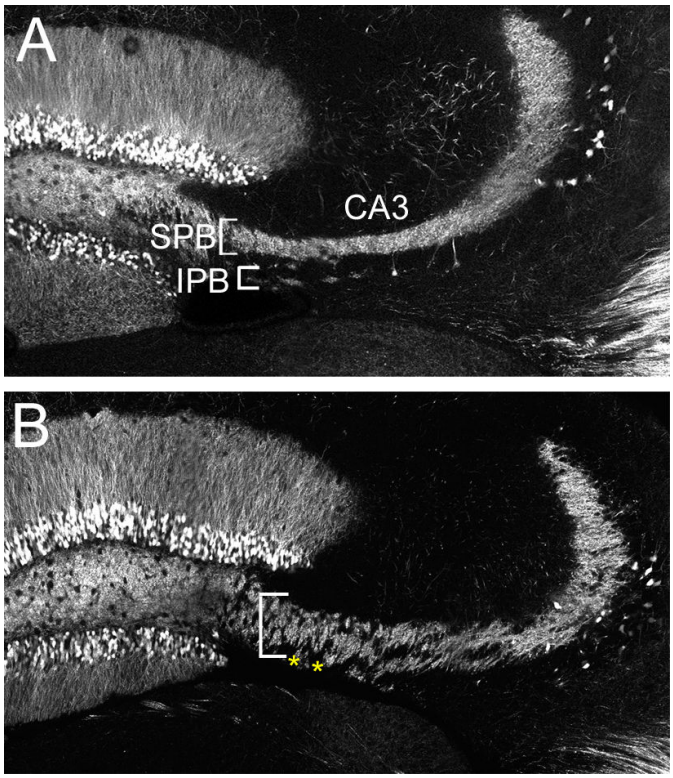

Figure 7. *Thy1-GFP* highlights structural deficits in the adult dentate gyrus

Staining shows mossy fiber projections in 4 month old control *Thy1-GFP/+;Tubb2b*$^{+/+}$ (A) and *Thy1-GFP/+;Tubb2b*$^{brdp/+}$ (B) animals in the CA3 region. Note that in the control animals there is both a suprapyramidal bundle (SPB, white brackets) and an infrapyramidal bundle (IPB, yellow arrow heads). In contrast, mossy fibers appear less dense and there is a lack of separation between the SPB and IPB in the *Tubb2b*$^{brdp/+}$ animals (asterisks).